

Article

Study on the Hydrogenation of Ethyl Stearate to the Fatty Alcohol 1-Octadecanol over Ru on Tungstated Zirconia

 Diego Quintero-Ramos, Manuel Checa, Jose Luis Jordá  and Maria J. Sabater * 

Instituto de Tecnología Química, Universitat Politècnica de València–Consejo Superior de Investigaciones Científicas, Avinguda dels Tarongers, s/n, 46022 València, Spain

* Correspondence: mjsabate@itq.upv.es

Abstract: Fatty alcohols are important products in the chemical industry, given that they are frequently used in the formulation of surfactants and lubricants. In this context, this work describes a catalytic heterogeneous approach for the production of 1-octadecanol (C₁₈OH) from ethyl stearate (ES) using nanosized Ru-supported on tungstated zirconia (W/Zr). The activity and selectivity of this series of catalysts have been studied during the hydrogenation of ES in a batch reactor at 175 °C and P_{H₂} = 40 bar. The so-prepared catalysts were characterized by a sort of characterization techniques (i.e., X-ray diffraction, H₂-TPR, etc.), confirming the high dispersion and higher reducibility of Ru nanoparticles on the W/Zr surface (primarily tetragonal zirconia) with respect to pure zirconia. Overall, the catalysts were significantly active. In addition, a strong synergistic effect was revealed between Ru and W species, according to catalytic data. Finally, the reaction sequence towards fatty alcohol has also been elucidated, pointing to the ester hydrogenolysis to the aldehyde and ulterior hydrogenation of the latter as the main route for fatty alcohol formation.

Keywords: fatty ester; fatty alcohol; ruthenium; zirconia; tungsten; hydrogenation



Citation: Quintero-Ramos, D.; Checa, M.; Jordá, J.L.; Sabater, M.J. Study on the Hydrogenation of Ethyl Stearate to the Fatty Alcohol 1-Octadecanol over Ru on Tungstated Zirconia. *Catalysts* **2023**, *13*, 1362. <https://doi.org/10.3390/catal13101362>

Academic Editor: Ken-ichi Fujita

Received: 23 August 2023

Revised: 29 September 2023

Accepted: 9 October 2023

Published: 11 October 2023

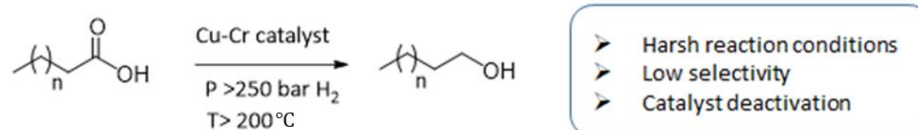


Copyright: © 2023 by the authors. Licensee MDPI, Basel, Switzerland. This article is an open access article distributed under the terms and conditions of the Creative Commons Attribution (CC BY) license (<https://creativecommons.org/licenses/by/4.0/>).

1. Introduction

Fatty alcohols are straight-chain primary alcohols whose origin can be both synthetic or natural and are highly appreciated for having important applications as indispensable intermediates for the production of lubricants, the plasticizer industry (between six and ten carbon atoms), the detergent industry (more than eleven carbon atoms), cosmetics, food additives, pharmaceuticals, industrial solvents, etc.

In this context, the hydrogenation of fatty acids to their corresponding alcohols is considered an important industrial task due to the broad use of fatty alcohols in important fields of specialty chemicals, as stated [1–3]. Nonetheless, although fatty acids are an abundant worldwide commodity, most alcohol producers think it preferable to hydrogenate the corresponding fatty acid esters (FAEs). This is due in part to the difficulty of directly hydrogenating acids due to the required harsh reaction conditions (i.e., temperatures and H₂ pressure above 200 °C and 250 bar, respectively), low selectivity, and the sensitivity of many catalysts to acids (Scheme 1) [4].



Scheme 1. Large-scale hydrogenation of fatty acids to fatty alcohols.

In sharp contrast, hydrogenation of FAEs can be carried out at lower temperatures, as evidenced by a variety of efficient homogeneous metal-catalyzed ester hydrogenations under mild conditions that have been recently reported [5–13]. In this regard, owing to

their lower expense, renewability, eco-friendliness, and biodegradability, priority is being given to obtaining them from greasy wastes (i.e., mainly from the hydrogenation of vegetal and animal fats) [14–17].

To summarize briefly, during the 80s, different companies designed their own slurry processes for the hydrogenation of methyl esters and fatty acids (via waxes) to produce fatty alcohols using different versions of a copper chromite catalyst [18–20]. Subsequently, fixed-bed reactors were also reported, which operated at high H₂ pressure. For example, the Air-Liquide (Lurgi) technology had an operating procedure at 250 bar pressure in a liquid phase process, while the Davy process was taking place in the vapor phase at 40 bar pressure [21]. In addition, and as information of interest, the pioneering Adkins (CuO/CuCr₂O₄) catalysts are still used to manufacture fatty alcohols on an industrial scale with yields in excess of 90% [22,23].

Given these precedents, it seems that the large-scale hydrogenation of FAEs has hardly changed over the past decades since it still basically takes place with the intervention of Cu/Cr catalysts under reaction conditions ranging from 25 to 30 MPa hydrogen pressure and 200–300 °C temperature [24].

In this regard, not only the harsh reaction conditions but the toxic nature of chromium render these catalysts unsuitable for extensive use from a green point of view. For this reason, the development of efficient Cr-free catalysts as a green alternative for producing fatty alcohols is highly desirable. Efforts have been invested in obtaining highly active and selective Cr-free catalysts, many of them based on Cu (i.e., mono and bimetallic Cu-based catalysts such as Cu-Zn, CuO/ZnO/Al₂O₃, Cu-Fe, Cu-Zn-Al-Ba mixed oxide, etc.) and noble metals [25–32], and, more recently, with Ni and Co-based catalysts [33–37].

Although in some cases, the selectivities and conversions achieved were very high, and in many cases, the reaction conditions were still very demanding (i.e., T > 250 °C and P_{H₂} > 5 MPa). In parallel, different Ru-based catalysts using different promoters (i.e., B, Sn, Ge, etc.) were also reported. In this case, the Ru activity was substantially reduced in the presence of Sn, although conversion and selectivity improved (>98%) for producing the fatty alcohol derived from methyl oleate [38,39].

Following this line, in this study, a series of supported Ru-based catalysts has been developed to be applied as catalysts in the hydrogenation of ethyl stearate (ES) to 1-octadecanol or stearyl alcohol (C₁₈OH). Stearic acid (also denoted as octadecanoic acid) is found mostly in animal fats as a mixed triglyceride and as an ester of fatty alcohol and is frequently used in cosmetics, plastics, stiffening detergents, and soaps [40].

In this case, Ru has been deposited on ZrO₂, given the interest that this oxide has aroused over the past decades due to a large number of catalytic applications in the industry [41]. Then, modification with the high valent element, Wⁿ⁺, has also been addressed, given that tungstated oxides show less tendency to deactivation and superior stability than other strong solid acids (i.e., sulfated oxides) under both oxidizing and reducing conditions [42–45]. Then, an H₂-TPR study has shown that W facilitates the reducibility of all Ru species, whereas an adequate Ru/W ratio will enhance the hydrogenating activity of the catalyst through an appreciable cooperative effect. Interestingly, such a synergistic effect has been related to the formation of WO₃ species.

2. Results and Discussion

2.1. Structural Characterization of Synthesized Catalysts

Zirconia was synthesized according to a method reported in the literature (see Section 3.2). In this case, X-ray powder diffraction (XRPD) analysis of the synthesized supports revealed that a mixture of crystalline tetragonal (2θ = 30.24, 34.80, 50.70) and monoclinic (2θ = 28.18, 31.40, 34.2, 35.3) ZrO₂ phases had formed (t-ZrO₂ and m-ZrO₂, respectively) (Figure 1A) [46,47]. Then, Ru metal was incorporated, as described in Section 3.2, to give the solid Ru(1)/ZrO₂. In this case, structural analysis by XRPD confirmed the stability of the ZrO₂ phase and the absence of segregated phases derived from Ru (Figure 1B).

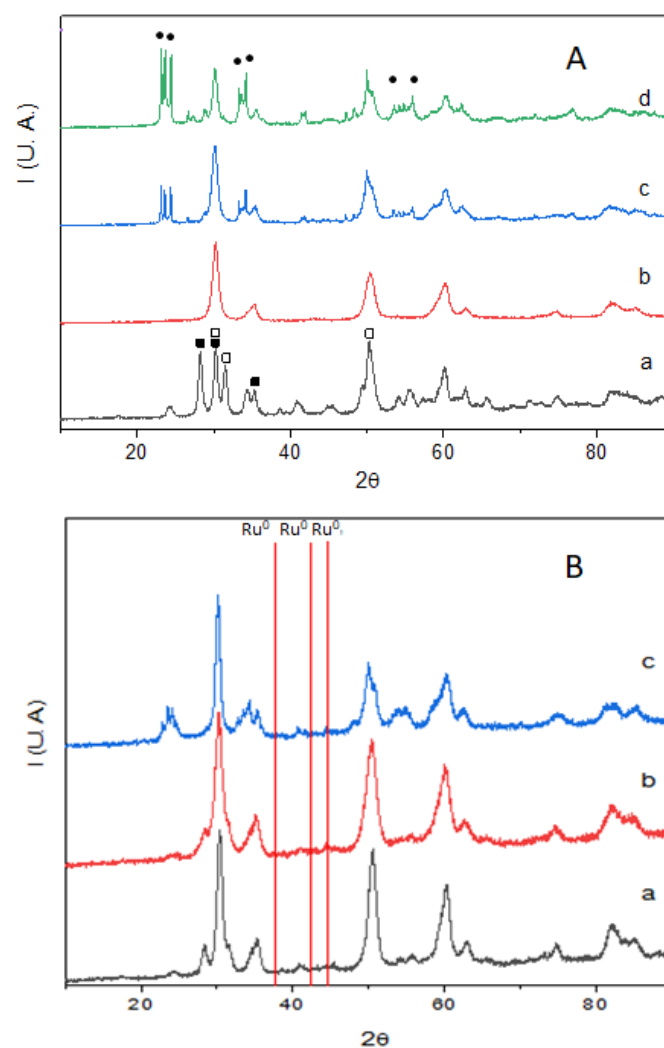


Figure 1. (A) XRP diffractograms obtained for pure zirconia and W/Zr mixed oxides with increasing amounts of W, highlighting the ZrO₂ and WO_x phases: (a) ZrO₂, (b) W(20)/Zr, (c) W(33)/Zr, (d) W(50)/Zr. Crystalline phases identified: *m*-ZrO₂ (■) and *t*-ZrO₂ (□) and WO₃ (●); (B) X-ray diffraction patterns of Ru-doped ZrO₂ (Ru/Zr) and Ru-doped ZrO₂ with increasing amounts of WO_x (Ru/W/Zr) in the 10 to 90° 2θ range: (a) Ru(1)/Zr, (b) Ru(1)/W(12)/Zr, and (c) Ru(1.3)/W(33)/Zr.

At this point, given that the incorporation of Sn⁴⁺ improved the selectivity towards obtaining oleyl alcohol during the hydrogenation of the corresponding fatty acid over Ru supported on alumina [48,49], a study about the influence of Wⁿ⁺ was carried out.

For this, a series of tungstated zirconias (i.e., W/Zr) was prepared from W deposition on zirconium oxyhydroxide using increasing proportions of W (see Section 3.2). Both the structure and physico-chemical characteristics of the resulting solids were analyzed by X-ray diffraction as well as by typical surface characterization techniques. In principle and as a curiosity, the diffractograms showed that the incorporation of W on ZrO₂ stabilized the crystallization of metastable tetragonal ZrO₂ (*t*-ZrO₂) over monoclinic ZrO₂ phase (*m*-ZrO₂) [41]. In close connection to this, there are precedents in the literature indicating that the stabilization of the tetragonal polymorph occurs under mild temperature and pressure conditions when an iso- or aliovalent zirconium substitution of larger cationic radii takes place (i.e., Y⁴⁺, Ga³⁺, Gd³⁺, and Fe³⁺) [50–52].

On the other hand, it is important to indicate that the formation of WO₃ (2θ = 23–25°) was detected from a tungsten content of about 33 wt.% (Figure 1). In this regard, early studies have shown that there is a maximum amount of WO_x on ZrO₂ before crystalline WO₃ is formed. According to these studies, there is a dispersion threshold where WO_x

species are considered to cover the surface of ZrO_2 in a monolayer state [46,53]. Calculations of different models have shown that the dispersion (or W surface density) (ρ) threshold should be around 6–8 W atoms/ nm^2 . Then, when the W surface density is below this value, W usually will exist in the form of isolated monotungstate species. However, when the W surface density is close to the dispersion threshold, WO_x will form polytungstate species and, finally, the crystallized WO_3 nanoparticles (W NPs) [46,54].

In our case, we have calculated the tungsten surface density (ρ) for W(33)Zr (the support of one of the most active catalysts, as will be seen later) as 18.9 W atoms/ nm^2 , which is well above the dispersion threshold. So, in principle, under these conditions, there might surely be polytungstate species as well as WO_3 species (detected by X-ray diffraction) [54].

In summary, the incorporation of about 20 wt.% of W led to the stabilization and exclusive formation of *t*- ZrO_2 , whereas an increase of up to 33 wt.% W led to the detection of WO_3 species according to diffraction data. All these features will have an influence on the catalysis, as will be shown later.

Continuing with this study, it is important to remark that the characteristic peaks of ZrO_2 and WO_3 were not affected by the deposition of Ru (Figure 1), not even when the Ru content was increased to twice the original (Ru 2 wt.%), as could be deduced from Figure S1 (see Supplementary Materials). In fact, for both Ru(1.3)/W(33)Zr and Ru(2)/Zr(33)W catalysts, only the typical reflections of ZrO_2 were observed in the corresponding diffractograms.

In this case, the absence of characteristic diffraction peaks of the ruthenium crystallites (even with a content of up to 2 wt.%) was interpreted as proof of good metallic dispersion on the W/Zr surface (Figure S1).

For the purposes of comparison, TiO_2 was also used as support. Figure S2 shows the diffractograms obtained for two analogous Ru-based catalysts supported on the mixed oxide W/Ti (Ru/W/Ti) and pure TiO_2 taken as a reference (see details for its synthesis in Section 3.2). In both cases, the characteristic peaks of WO_3 ($2\theta = 23\text{--}25^\circ$) and titania in the anatase phase ($2\theta = 25.2, 37.9, 48.1$) were observed [55].

Given that, as in the previous case with zirconia, no peaks that could be attributed to a Ru phase ($2\theta = 42.0$) could be detected by XRPD, this was again interpreted as a probe of a good metallic dispersion on the titania surface.

2.2. Physico-Chemical and Textural Characterization of Synthesized Catalysts

Nitrogen adsorption/desorption isotherms were used to investigate the Brunauer, Emmett, and Teller (BET) surface area and pore volume, whereas average metal particle size and distribution of elements on the surface was determined by transmission electron microscopy (TEM). It is necessary to indicate that the analytical determination of each element was carried out by ICP-AES analysis and, in some cases, by X-ray fluorescence spectroscopy. The main chemical and textural characterization results obtained for this series of catalysts are included in Table 1.

In general, it was observed that the total pore volume and external surface area decreased as the W content on ZrO_2 increased (Table 1). The same observation took place with increasing amounts of Ru (Table 1).

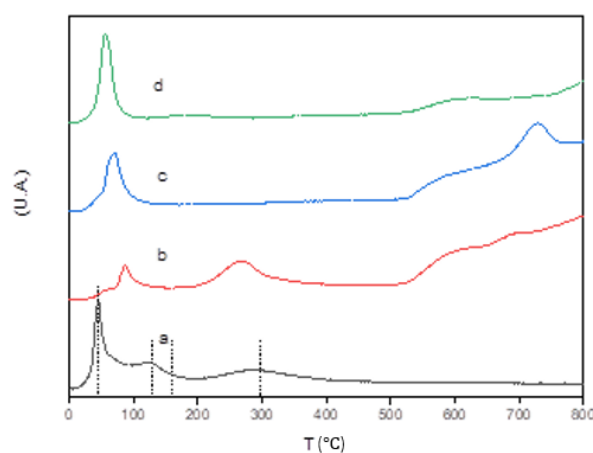
The metal particle size was determined through transmission electron microscopy (TEM). In this case, a dependence of the metal particle size with respect to the metal loading was observed. As an example, the catalyst Ru(0.5)/W(33)/Zr with a Ru load of 0.5% had an average metal particle diameter of 0.5 nm (entry 6, Table 1), while the catalyst Ru(1.3)/W(33)/Zr (entry 7, Table 1) with a Ru content of 1.3 wt.% showed a particle size of about 1.2 nm.

Figures S3–S5 (see Supplementary Materials) show some of the most representative TEM micrographs of the catalysts from which the average diameter of the metal particles deposited on the different supports was determined. Then, the reducibility of the most representative Ru-based catalysts was also obtained as data of interest. Figure 2 illustrates the H_2 -TPR profiles of this series of Ru-based catalysts.

Table 1. Characterization results obtained by ICP-AES, X-Ray fluorescence spectroscopy, N₂ adsorption isotherms, and TEM.

Entry	Catalyst ^a M(x)/P(y)/S	Ru (wt.%)	%W (wt.%)	S _{BET} (m ² /g)	V _{pore} (cm ³ /g)	D(nm) ^b
1	ZrO ₂	-	-	195	0.18	-
1	W(12)/Zr ^c	-	12	112	0.17	-
2	W(33)/Zr ^d	-	33	57	0.15	-
3	W(50)/Zr ^d	-	50	25	0.06	-
4	Ru(1)/Zr	1	-	81	0.42	1.6
5	Ru(1)/W(12)/Zr ^d	1	-	76	0.34	0.9
6	Ru(0.5)/W(33)/Zr ^d	0.5	-	48	0.20	0.5
7	Ru(1.3)/W(33)/Zr ^d	1.3	-	40	0.20	1.2
8	Ru(2)/W(33)/Zr ^d	2	-	34	0.19	1.5
9	Ru(1)/W(30)/Ti ^d	1	-	7	0.05	1.6

^a M(x) = wt.% Ru; P(y) = wt.% W; S = Support; ^b Average metal particle size determined by transmission electron microscopy (TEM); ^c Analysis obtained by ICP-AES; ^d Analysis obtained by X-ray fluorescence spectroscopy.

**Figure 2.** H₂-TPR of catalysts: (a) Ru(1)/Zr, (b) Ru(0.5)/W(33)/Zr, (c) Ru(1.3)/W(33)/Zr and (d) Ru(2)/W(33)/Zr.

From Figure 2, it could be deduced that, in general, the incorporation of W on zirconia brought an improvement in the reducibility of Ru. Effectively, ruthenium on pure zirconia (Ru(1)/Zr) showed two reduction peaks at relatively low temperatures: (a) a reduction peak about 50 °C which was associated with the reduction of well-dispersed RuO_x species to metal; (b) a second reduction peak about 130 °C associated to the reduction of RuO_x nanoparticles with low dispersion (>3 nm); and (c) a third one around 300 °C, which was attributed to Ru species interacting strongly with the support through strong metal-support interactions (SMSI) [56].

It is important to indicate that in the presence of 33 wt.% W, the two most easily reducible Ru species (at 130 °C and 50 °C) evolved to give essentially a single more uniform metallic species that could be reduced at intermediate temperature (approx. 70 °C) (Figure 2a,b), whereas the reduction of SMSI species took place below 300 °C (Figure 2a,b). It is interesting to note that these SMSI species were undetectable with higher Ru loadings (1–2 wt.% Ru) (Figure 2c,d).

Finally, given that the reduction of the WO_x species took place from 550 °C (Figure 2), a reduction temperature of 400 °C was selected to guarantee the complete and exclusive reduction of surface Ru species when preparing the series of catalysts.

2.3. Catalytic Studies

The fatty alcohol production through the hydrogenation of fatty acid derivatives is an environmentally friendly process that can be complementary to the industrial one, which is

based on petrochemical processes. In this case, the hydrogenation of ethyl stearate (ES) to 1-octadecanol ($C_{18}OH$) was chosen as a model reaction to determine the activity/selectivity of the Ru-based catalytic systems thus prepared. In this case, a preliminary screening of reaction conditions led to determining the optimal experimental parameters: 175 °C, 40 bar hydrogen pressure, 1 mmol of ES, 0.6 mmol of n-dodecane (internal standard), 3 mL of hexane, and 100 mg of catalyst.

Then, the data collected in Table 2 shows the catalytic data obtained at different conversion values with the Ru-based solid catalyst series.

Table 2. Ethyl stearate (ES) hydrogenation with different Ru catalysts.

Reaction scheme: Ethyl stearate (ES) reacts with 100 mg catalyst, 40 bar H_2 , and 175 °C to produce 1-octadecanol ($C_{18}OH$), stearic acid (SA), steryl stearate (SS), and hydrocarbons C_{18} and C_{17} .

Entry	Catalyst ^a	C(%) ^b	t(h)	S(%) ^b		
				$C_{18}OH$ ^c ($C_{18}OH:SS$)	SA	[$C_{18}+C_{17}$] ^d ($C_{18}:C_{17}$)
2	Ru(0.5)/W(33)/Zr	30	15	80 (37:63)	3	17 (41:59)
		60	30	75 (19:81)	3	22 (45:55)
3	Ru(1.3)/W(33)/Zr	30	5	70 (100:0)	5	25 (52:48)
		60	12	71 (70:30)	3	26 (54:46)
4	Ru(2)/W(33)/Zr	30	2	61 (82:18)	4	35 (43:57)
		60	4	46 (74:26)	1	53 (43:57)
5	Ru(1)/W(12)/Zr	30	8	63 (75:25)	8	29 (31:69)
		60	22	62 (47:53)	1	37 (22:78)
6	Ru(2)/W(50)/Zr	30	15	70 (86:14)	4	26 (58:42)
		60	30	73 (53:47)	2	25 (60:40)
7	Ru(1)/W(30)/Ti	30	27	52 (100:0)	3	45 (71:29)

^a Reaction conditions: ES (1 mmol), n-dodecane (internal standard, 0.6 mmol), n-hexane (3 mL), catalyst (100 mg), P_{H_2} = 40 bar, T = 175 °C, 1000 rpm; ^b Conversions and selectivities in percentage (C(%) and S(%), respectively) were determined by GC using n-dodecane as internal standard and confirmed by GC-MS; ^c Selectivity (%) to $C_{18}OH$ was calculated by GC considering the free and esterified $C_{18}OH$ fraction in SS; ^d Selectivity (%) to long-chain hydrocarbons C_{18} (%) and C_{17} (%) was calculated by GC.

As can be deduced from Table 2, along with the desired fatty alcohol C₁₈OH, other secondary products were formed, such as SA, the transesterification product SS, and the straight chain hydrocarbons heptadecane and octadecane (C₁₇ and C₁₈, respectively).

It is interesting to note that the W-catalyzed acid hydrolysis to give SA was something unimportant, regardless of the content of W—a fact that was attributed to the effect of using a nonpolar solvent such as n-hexane (Table 2), which, in principle, would keep water away from the catalyst surface during the reaction, thus preventing ester hydrolysis [57,58].

If this were so, cleavage of the C-O bond through direct ester hydrolysis to produce an aldehyde intermediate could be the main route towards 1-octadecanol C₁₈OH, although we will return to this point later.

Regarding the transesterification reaction and in line with the need for acid catalysis to form SS [59], it was found that this secondary reaction was especially relevant with those catalysts with a high W content and low Ru content (i.e., entry 2, Table 2). Also, as might be expected, the selectivity towards SS increased in all cases with time at the expense of the formation of fatty alcohol.

Nonetheless, the most remarkable fact was that the formation of linear hydrocarbons C₁₇ and C₁₈ competed significantly with the formation of fatty alcohol C₁₈OH, presumably through (a) a decarbonylation reaction to give C₁₇ (b) and a hydrodeoxygenation HDO and/or a sequential dehydration/hydrogenation pathway to give C₁₈.

By analyzing these results by parts, the initial reaction rate (r_0) and TOF for forming C₁₈OH were calculated for the series of catalysts with different Ru content (0.5–2%) and the same proportion of W (entries 2–4, Table 2), and the obtained values were plotted against the Ru content (%) (Figure 3A).

According to Figure 3A, a linear dependence between catalytic activity and Ru content could be obtained by showing the following order of activity:



That is, the higher the Ru content (wt.%), the higher the proportion of fatty alcohol C₁₈OH obtained. In parallel, the influence of W as a promoter was also studied. To achieve this, three different catalysts with the same Ru content (approx. 1 wt.%) and variable amounts of W (0–33 wt.%) were selected (entries 1, 3, and 5, Table 2) (Figure 3B). Then, the catalytic data (r_0 and TOF for forming C₁₈OH) were obtained for these three catalysts, and the results were plotted versus the W content (wt.%). Interestingly, the graph in Figure 3B clearly showed that the catalytic activity for forming C₁₈OH increased exponentially with the W content, leading to a maximum with the catalyst Ru(1.3)/W(33)/Zr (entry 3, Table 2) and pointing to the existence of a plausible synergistic effect between Ru and W, which coincided with the formation of WO₃ according to X-ray diffraction data.

In addition, the selectivity values were also obtained at two different conversion values (30 and 60%) for the three catalysts included in Table 2 (entries 2–4), and these selectivity values were plotted against the Ru and W content (Figure 4).

Regarding the Ru content, a Gaussian-type curve was obtained in which the catalyst Ru(1.3)/W(33)/Zr gave the best selectivity values towards C₁₈OH at both low and high conversion values. Regarding the W content, it is interesting to note that the best selectivity values towards fatty alcohol were obtained with 33 wt.% W, coinciding again with the formation of WO₃ species according to X-ray diffraction data in Figure 1.

Then, with this information in hand, we tried to expand these catalytic studies to a different reducible oxide, such as TiO₂, given that the latter has a greatly recognized stability under similar reaction conditions.

Thus, a closely related Ru/W based catalyst was prepared on TiO₂ (P25) (Section 3.2), which was named Ru(1)/W(30)/TiO₂. The performance of this catalyst was compared with that of the previous catalyst Ru(1.3)/W(33)/Zr during the selective reduction of ES into the fatty alcohol C₁₈OH under the same experimental conditions (Figure 5).

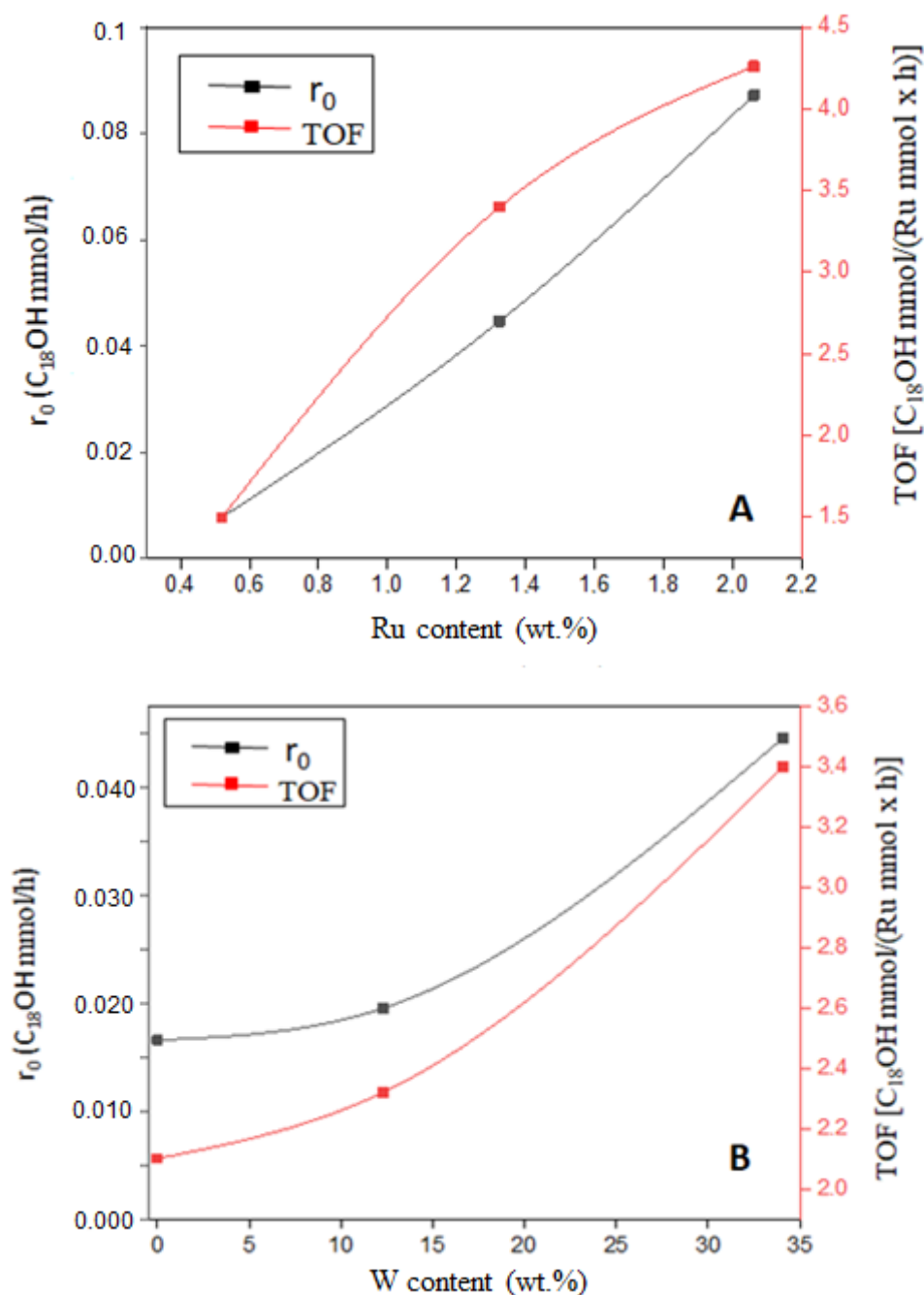


Figure 3. (A): Catalytic activity (r_0 and TOF values) for Ru-based catalysts with different Ru content and W (33 wt.%): Ru(0.5)/W(33)/Zr, Ru(1.3)/W(33)/Zr and Ru(2)/W(33)/Zr; (B) Catalytic activity (r_0 and TOF values) for catalysts with different W content and Ru (approx. 1 wt.%) [Ru(1)/Zr, Ru(1)/W(12)/Zr and Ru(1.3)/W(33)/Zr]. Reaction conditions: ES (1 mmol), n-dodecane (0.6 mmol), n-hexane (3 mL) and catalyst (100 mg), P_{H_2} = 40 bar, T = 175 °C, 1000 rpm.; TOF: mmol $C_{18}OH$ /mmol Ru \times h.

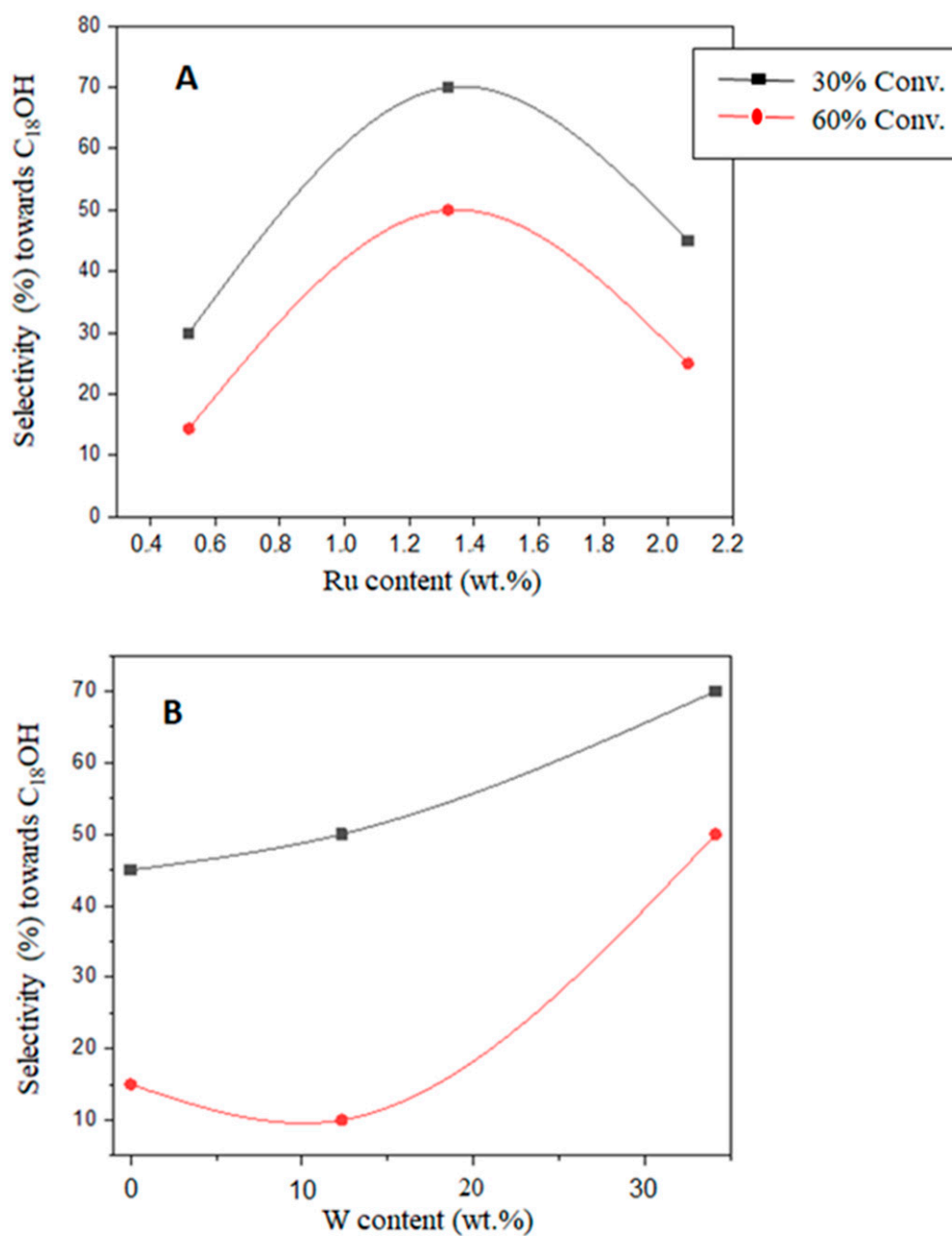


Figure 4. (A): Selectivity towards fatty alcohol C₁₈OH in the presence of catalysts containing increasing amounts of Ru and the same W content (33 wt.%): Ru(0.5)/W(33)/Zr, Ru(1.3)/W(33)/Zr, and Ru(2)/W(33)/Zr; (B) Selectivity towards fatty alcohol C₁₈OH in the presence of catalysts containing increasing amounts of W and the same Ru content (1 wt.%) [Ru(1)/Zr, Ru(1)/W(12)/Zr, and Ru(1.3)/W(33)/Zr]. Reaction conditions: ES (1 mmol), n-dodecane (0.6 mmol), n-hexane (3 mL) and catalyst (100 mg), P_{H₂} = 40 bar, T = 175 °C, 1000 rpm.

Interestingly, although in both cases, the selectivity towards C₁₈OH was rather similar during the first stages of the reaction (Table 2), Ru(1.3)/W(33)/Zr was much more active than Ru(1)/W(30)/Ti, hence stressing the importance of the support (Figure 5).

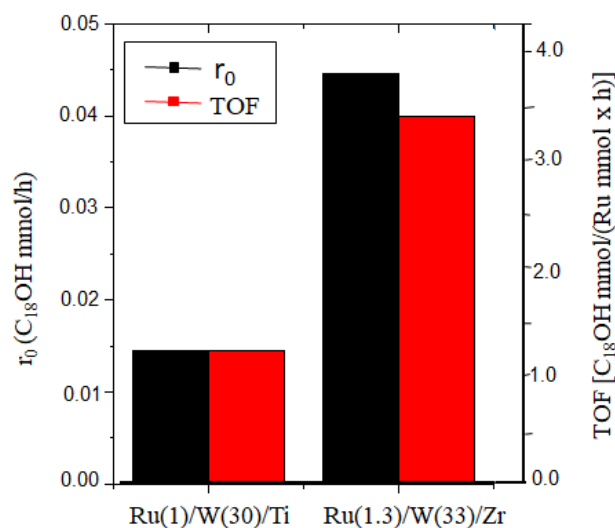


Figure 5. Catalytic activity during the first stages of reaction (r_0) and TOF values during the hydrogenation reaction of ES to give C₁₈OH in the presence of Ru(1)/W(30)/Ti and Ru(1.3)/W(33)/Zr catalysts at 30% isoconversion. Reaction conditions: ES (1 mmol), n-dodecane (0.6 mmol), n-hexane (3 mL), catalyst (100 mg); P_{H₂} = 40 bar, 175 °C at 1000 rpm; TOF: mmol C₁₈OH/mmol Ru × h.

2.4. Mechanistic Studies

A priori, the formation of 1-octadecanol C₁₈OH via hydrogenation of the fatty ester, ES, can be the consequence of a double hydrogenation of the latter, first to the aldehyde octadecanal and then to the corresponding fatty alcohol C₁₈OH.

However other non-desired products were also formed: (a) a minor product derived from acid hydrolysis of the fatty ester named SA, which could also participate in the production of fatty alcohol; (b) the transesterification product SS; (c) the decarbonylation product heptadecane C₁₇ (A control reaction was carried out to confirm that heptadecane C₁₇ came from the decarbonylation of 1-octadecanol [Reaction conditions: 175 °C, P_{H₂} = 40 bar, C₁₈OH (1 mmol), n-dodecane as internal standard (0.6 mmol), hexane (3 mL), Ru(1.3)W(33)/Zr catalyst (100mg)]. In this case C₁₈OH was transformed into long chain hydrocarbons C₁₇ and C₁₈); and (d) octadecane C₁₈—which could form surely through a sequential dehydration/hydrogenation reaction of C₁₈OH as main reaction pathway [60].

This last hypothesis was supported by the fact that the decarbonylation product C₁₇ predominated over C₁₈ in the presence of Ru(1)/Zr as a catalyst (entry 1, Table 2). However, the surface acidity introduced by W could make the dehydration /hydrogenation pathway from C₁₈OH become highly favored (through a plausible and undetected alkene intermediate) [60–62], making this pathway compete efficiently with decarbonylation, thus giving a more balanced ratio of both hydrocarbons (C₁₇ and C₁₈) (entries 2–6, Table 2).

Figure 6 displays the evolution of selectivity for different products with time in the presence of Ru(1.3)/W(33)/Zr as a catalyst.

When looking carefully at the evolution of reaction with time from Figure 6, it can be observed that the selectivity towards the fatty alcohol gradually increased over time, reaching a maximum selectivity of 70% after 3 h, then decreasing at the expense of the transesterification product SS and the long chain hydrocarbons C₁₇ and C₁₈.

Along with these observations and in order to aid in the elucidation of the reaction scheme, the following control reactions were run in parallel:

- The free carboxylic acid SA was put in contact with Ru(1.3)/W(33)/Zr under H₂ (P = 40 bar) at 175 °C, being rapidly transformed into the long-chain hydrocarbons C₁₈ and C₁₇, through the intermediation of fatty alcohol C₁₈OH. In no case was the formation of aldehyde detected. However, given that SA was always a minority and tended to decrease with time (Figure 6), we inferred that the main route towards

- $C_{18}OH$ could be very likely the ester hydrogenolysis followed by reduction of the resulting aldehyde and not the hydrogenation of SA (see Scheme 2 below).
- (b) A long-chain aldehyde was taken as an aldehyde model (i.e., decanal), being contacted with Ru(1)/W(33)/Zr under the same experimental conditions. In this case, the aldehyde was rapidly transformed into the long-chain paraffins C_{10} and C_9 in less than 10 min, giving a product distribution equivalent to that obtained starting from the fatty acid SA. Thus, this experimental fact confirmed that the aldehyde, although it is never detected, is more certainly the key intermediate in the transformation into fatty alcohol and paraffin.
- (c) In addition, $C_{18}OH$ was also transformed exclusively into the same C_{17} and C_{18} hydrocarbons in the presence of Ru(1.3)/W(33)/Zr as a catalyst (A control reaction was carried out to confirm that heptadecane C_{17} came from the decarbonylation of 1-octadecanol [Reaction conditions: 175 °C, P_{H_2} = 40 bar, $C_{18}OH$ (1 mmol), n-dodecane as internal standard (0.6 mmol), hexane (3 mL), Ru(1.3)W(33)/Zr catalyst (100mg)]. In this case $C_{18}OH$ was transformed into long chain hydrocarbons C_{17} and C_{18}).

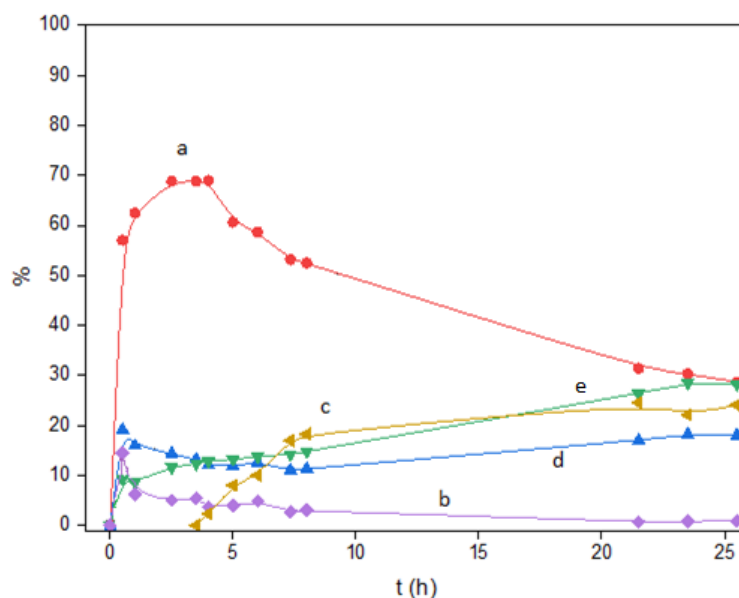
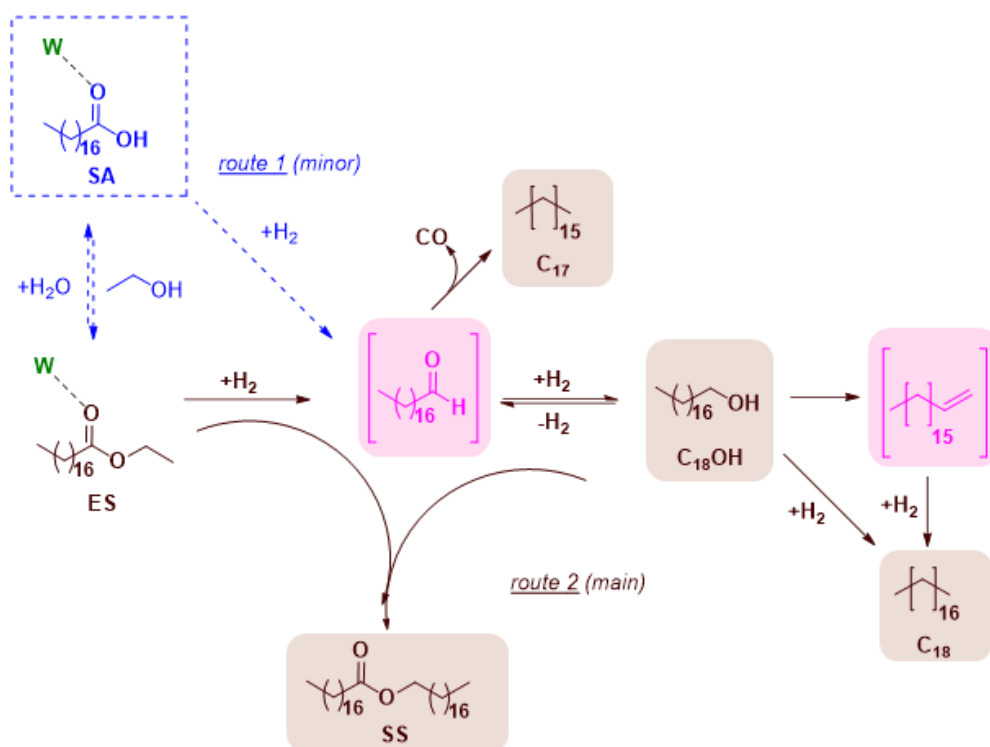


Figure 6. Transformation of ES into $C_{18}OH$ catalyzed by Ru(1.3)/W(33)/Zr: (a) Selectivity (%) to $C_{18}OH$ calculated by GC; (b) Selectivity (%) to SA calculated by GC; (c) Selectivity (%) to SS obtained by GC; (d) Selectivity (%) to n-heptadecane C_{17} calculated by GC; (e) Selectivity (%) to n-octadecane C_{18} calculated by GC. Reaction conditions: ES (1 mmol), n-dodecane (0.6 mmol), n-hexane (3 mL) and catalyst (100 mg), P_{H_2} = 40 bar, T = 175 °C, 1000 rpm.

Thus, from these results and in order to explain the formation of $C_{18}OH$ and the set of secondary products detected during the hydrogenation of ES, the following reaction scheme could be established:

In accordance with this, the most efficient catalytic system (Ru(1.3)W(33)/Zr) achieved 100% selectivity for 1-octadecanol under mild conditions (175 °C and 4.0 MPa of H_2) at low and moderate conversion levels (Table 2). Here, a metal-Lewis acid cooperation between Ru/W was primarily responsible for the high activity towards 1-octadecanol or stearyl alcohol $C_{18}OH$, something that could be evidenced by a significant exponential increase in the initial reaction rate (r_0) and the TOF for obtaining the fatty alcohol with the addition of W (Figure 3). To explain this experimental result, it is necessary to take into account that hydrogenation of carbonyl groups can take place through (a) the homolytic cleavage of H_2 , with supported transition metal catalysts [63,64], as well as (b) a heterolytic cleavage (dissociation of H_2 into H^- and H^+), where the metal bonds to a Lewis base to form a metal-base pair (i.e., catalysts based on metals immobilized on oxidic supports, like those of this study) [65].



Scheme 2. Plausible reaction scheme during the hydrogenation reaction of ES with the Ru-based catalyst Ru(1.3)W(33)/Zr.

In this regard, we foresee that the acidity of the catalyst could facilitate the reaction through a heterolytic dissociation. That is, the interaction of the ester group with W can cause a weakening or activation of the C=O bond, hence making the attack on the carbonyl group by the metal hydride (H^-) much easier. At the same time, the protonation (H^+) of the leaving alkoxy group would also be facilitated under acidic conditions, giving rise to the formation of the corresponding alcohol (Scheme 2).

It is important to highlight that the introduction of acidity by the W was not enough for the ester hydrolysis reaction to be competitive, so the formation of fatty alcohol from the hydrogenation of SA remained as a minority route (route 1, Scheme 2). In this regard, we assumed that ester hydrogenolysis, followed by aldehyde hydrogenation, was the main route towards the fatty alcohol (route 2, Scheme 2). Finally, we obtained that the catalyst was stable under the reaction conditions since it could be used up to three times with no appreciable loss of activity and selectivity to 1-octadecanol.

3. Materials and Methods

3.1. Reagents and Chemicals

All reagents and solvents used in this study: NaOH, $NaBH_4$, $ZrOCl_2 \cdot 8H_2O$, NH_4OH/NH_4Cl buffer, $(NH_4)_6H_2W_{12}O_{40}$, $(NH_4)_8Mo_7O_{24}$, N,O-Bis(trimethylsilyl) trifluoroacetamide, n-hexane, n-dodecane, n-decane, n-nonane, 1-decanal, 1-decanol, n-heptadecane, n-octadecane, ethyl stearate (ES), octadecan-1-ol ($C_{18}OH$), stearic acid (SA), stearyl stearate (SS), and TiO_2 were supplied by Sigma-Aldrich (Merck KGaA, Darmstadt, Germany) and were used without any further purification.

3.2. Synthesis of Catalysts

3.2.1. Synthesis of ZrO_2 and Mixed Oxides $WZrO_x$ (W/Zr) and $WTiO_x$ (W/Ti)

Synthesis of ZrO_2

Zirconia was synthesized following the procedure described in the literature with slight modifications [66,67]. That is, 23.52 g of $ZrOCl_2$ were added to 135 mL Milli-Q[®]

EQ 7000 system (Merck KGaA, Darmstadt, Germany) H₂O (solution A). In parallel, 150 mL of a commercial NH₄OH/NH₄Cl (2 M) buffer solution (pH = 10–11) was prepared (solution B). Solution A was added dropwise over solution B under constant stirring, and the mixture was stirred at room temperature for 30 min. The white solid thus obtained was filtered off and washed with water MilliQ until chloride ions were completely removed. The obtained solid was resuspended in 150 mL of a 2 M NH₄OH/NH₄Cl buffered solution at pH = 10.5 and heated under reflux for 12 h at 90 °C with constant stirring. The resulting solid was filtered and washed again with abundant water until the chloride ions present were completely removed. Finally, the solid was dried in an oven for 12 h at 100 °C.

Synthesis of W/ZrO_x support (W/Zr)

A certain amount of zirconia (1 g) prepared according to the procedure previously described was impregnated with an aqueous solution (3 cm³/g ZrO₂) containing the required amount of ammonium metatungstate (NH₄)₆H₂W₁₂O₄₀ to obtain the desired amount of W on the solid surface. The resulting mixture was magnetically stirred for 12 h at 60 °C. Then, water was removed by heating to 60 °C under reduced pressure. The solid thus obtained was dried in an oven at 100 °C for 12 h, and then it was calcined under air (air flux: 10 mL/min) at 700 °C for 7 h (heating ramp of 10 °C/min and the time needed to reach 700 °C). The catalysts were synthesized with a nominal value of 12, 33, and 50 (wt.%) of tungsten. The amount of W is indicated in parentheses (i.e., W(33)/Zr).

Synthesis of WTiO_x support (W/Ti)

The same experimental procedure followed to support W on ZrO₂ was used to deposit W on TiO₂ (TiO₂ anatase phase). The catalysts were synthesized with 30 wt.% of tungsten. The amount of W is indicated in parentheses (i.e., W(30)/Ti).

3.2.2. Synthesis of Ru Supported on ZrO₂ (Ru/Zr)

1 g of calcined support ZrO₂ was suspended in 30 mL of distilled water with the aid of ultrasounds (EMAG Technologies, Ann Arbor, MI, USA) (30 min). Then, 1 mL of an aqueous solution containing the required amount of RuCl₃ (i.e., 23.84 × 10⁻³ or 62 × 10⁻³ or 95.35 × 10⁻³ mg RuCl₃) was added to obtain the desired ruthenium content (i.e., 0.5, 1.3, and 2 wt.% Ru) on the solid surface. The mixture was stirred while sodium hydroxide solution (0.1–1 M) was added dropwise until reaching pH = 13, being stirred further for 1 h under these conditions. The resulting solid was then separated by centrifugation and washed abundantly with distilled water to completely remove the chloride ions. The solid was dried in an oven at 60 °C for 12 h. Then, the solid was reduced at 400 °C for 3 h with H₂ flow (20 mL/min). The heating ramp was 10 °C/min, the time necessary to reach 400 °C. Cooling was performed using a 100 mL/min N₂ flow. The catalysts were synthesized with 1% (wt.%) of the metal. The amount of Ru is indicated in parentheses (i.e., Ru(1)/ZrO₂).

3.2.3. Synthesis of Ru Supported on WZrO_x and WTiO_x (Ru/W/Zr and Ru/W/TiO₂)

1 g of calcined W/Zr oxide (or W/TiO₂) was suspended in 30 mL of distilled water with the aid of ultrasounds (for 30 min). Then, 1 mL of an aqueous solution with the required amount of RuCl₃ was added to obtain the desired ruthenium content on the catalyst surface. The resulting slurry was stirred while sodium hydroxide solution (0.1–1 M) was added dropwise until reaching pH = 13, being stirred additionally for 1 h under these conditions. The resulting solid was separated by centrifugation, being washed abundantly with distilled water to completely remove chloride ions. The resulting solid was dried in an oven at 60 °C for 12 h, and then it was reduced at 400 °C for 3 h with H₂ flow (20 mL/min). In this case, a heating ramp of 10 °C/min was used until reaching the required temperature. Cooling was performed using a 100 mL/min N₂ flow.

3.3. Characterization of Catalysts

X-ray powder diffraction (XRPD) patterns were collected using a PANalytical CUBIX X-ray diffractometer (Malvern Panalytical, Sucursal B.V., Madrid, Spain) equipped with

Cu K α radiation ($\lambda = 1.5419$ nm) and fixed divergence slits in the 2θ range from 3.5 to 90° . The crystallite size of the zirconia phase was calculated from the X-ray powder diffraction patterns by means of the Scherrer equation, using the peak at 30.2° (2θ). The values obtained were very similar, and around 100 Å, in all the samples: Ru1Zr (109 Å), Ru1W12Zr (80 Å), Ru1W33Zr (99 Å), Ru0.5W33Zr (98 Å), and Ru2W33Zr (99 Å).

According to a semi-quantitative Rietveld analysis of the patterns, the samples with the lowest W contents (Ru1Zr and Ru1W12Zr) consisted of tetragonal and monoclinic (Baddeleyite) zirconia ($57/43$ and $56/44$ wt.%, respectively). The possible presence of a certain amount of cubic zirconia could not be completely excluded due to its large peak overlap with the tetragonal phase. The samples with the highest contents of W (Ru0.5W33Zr, Ru1W33Zr, and Ru2W33Zr) only presented the tetragonal zirconia phase, with no observable presence of the monoclinic one. In these three samples, the presence of monoclinic WO_3 was detected (approximately 75 wt.% ZrO_2 and 25 wt.% WO_3).

The chemical compositions of the samples were measured by Inductively Coupled Plasma-Atomic Emission Spectroscopy (ICP-AES) analysis. These analyses were carried out in a Varian 715-ES ICP Optical Emission spectrometer (Palo Alto, CA, USA). Solids were dissolved in HNO_3/HCl (1:3) + $\text{H}_2\text{O}_2/\text{H}_2\text{SO}_4$ aqueous solution or in a $\text{HNO}_3/\text{HCl}/\text{HF}$ aqueous solution.

Energy Dispersive X-ray Fluorescence or EDXRF was used to quantify the elements on those catalysts that did not dissolve with different mixtures of acids (i.e., aqua regia or $\text{HNO}_3/3\text{HCl}$). These fluorescence measurements were performed with a PANalytical MiniPal4 spectrometer (Malvern Panalytical, Malvern, UK) on the solid powder samples without any pretreatment. For this, a calibration line was obtained from standards prepared in the laboratory, using mixtures of WO_3 , ZrO_2 , and ruthenium(III) oxide (99.9%) in different proportions.

The average size and size distributions of the metal nanoparticles were measured by high-resolution transmission electron microscopy (HR-TEM) using a JEOL JEM 2100F microscope (Tokyo, Japan) operating at 200 kV both in transmission (TEM) and scanning-transmission mode (STEM). The equipment includes an EDS X-Max 80 detector (Oxford Instruments, Abingdon, UK) with a 127 eV resolution for chemical characterization and a high-angle annular dark-field (HAADF) detector. Samples were prepared by dropping the suspension of the material using CH_2Cl_2 as the solvent directly onto carbon-coated copper grids for transmission electron measurements. The mean particle sizes were estimated from HR-TEM micrographs by single-particle measurements of a determined number of particles.

The mean metal particle diameter was considered on the basis of its homogeneity, dispersion, and number of particles. The average particle size was estimated considering the surface distribution calculations:

$$D_p = \sum n_i d_i^2 / \sum n_i d_i^3 \quad (1)$$

where d_i is the measured diameter of the i th particle and n_i is the number of particles with this diameter.

Textural properties were determined from the adsorption–desorption isotherms of nitrogen, recorded at -196 °C with a Micromeritics ASAP 2420 (Micromeritics, Norcross, GA, USA). The specific area was calculated by applying the BET method to the relative pressure (P/P_0) range of the isotherms between 0.03 and 0.3 and taking a value of 0.162 nm² for the cross-section of an adsorbed nitrogen molecule at -196 °C. Pore size distributions were computed by applying the BJH model to the desorption branch of the nitrogen isotherms.

The samples were pressed at 5 tons of pressure, ground, and sieved until reaching a particle size between 0.4 and 0.6 mm. After this, the samples were subjected to degassing at 400 °C for several hours to ensure that no adsorbed molecules were found on the surface of the solid. A Micromeritics ASAP 2420 equipment was used.

TPR measurements were performed by using a Micromeritics AutoChem 2910 instrument (Micromeritics, Norcross, GA, USA) equipped with a thermal conductivity detec-

tor. For this, a known mass (approximately 200 mg) of the as-prepared reduced catalyst (Section 3.2.2) was pretreated under airflow (10 mL/min) at 723 K for 1 h. The sample was allowed to cool to room temperature, and then air was replaced by Ar for 15 min. Then, a reducing gas mixture (5% H₂/Ar) was passed at room temperature with a constant flow of 20 mL/min. Once the system was stabilized, the temperature was increased linearly up to 1073 K using a heating ramp of 10 K/min.

The reduction signal was calibrated by using the complete reduction of a standard CuO powder (Sigma-Aldrich; Merck KGaA, Darmstadt, Germany, 99.995%).

3.4. Catalytic Reactions: Hydrogenation of Ethyl Stearate (ES) to 1-Octadecanol (C₁₈OH)

Catalytic tests were carried out in a 15 mL stainless-steel reactor (Mecanizados Umesal, Valencia, Spain) equipped with a manometer and a micro-sampling system, which allowed the extraction of samples at regular reaction times with magnetic stirring.

The catalytic activity was studied using the hydrogenation reaction of ethyl stearate (ES) to octadecan-1-ol (C₁₈OH) or stearyl alcohol as a model reaction. In a typical reaction, hexane (5.6 mL), ES (1.2 mmol), catalyst (100 mg), and n-dodecane (0.60 mmol) as an internal standard were added to the reactor. The reactor was purged with H₂ and then pressurized to 40 bar. Once the desired reaction temperature was reached (175 °C), the reaction mixture was stirred at 1000 rpm for 24 h maximum.

The reaction was periodically monitored through gas chromatography using an HP-5 capillary column (5% phenylmethylsiloxane, 30 m × 320 μm × 0.25 μm). Products were identified by GC-MS using an Agilent (Santa Clara, CA, USA) 6890N8000 equipped with a mass spectrometry detector (Agilent 5973N quadrupole detector).

Sampling was performed by taking 25 μL of the reaction mixture and adding it into a vial containing 1 mL of n-hexane. Then, 160 mg of N,O-Bis(trimethylsilyl)trifluoroacetamide and 30 μL of pyridine were added, and the vial was stoppered and heated (80 °C) for 10 min. Afterwards, it was allowed to cool to room temperature, and the sample was injected into the gas chromatograph (Agilent Technologies, Madrid, Spain). The equipment used was an "Agilent 7890" with an FID flame ionization detector. The column used was a 30 m long and 0.25 μm thick HP-5 capillary filled with phenylmethylsiloxane (5%).

3.5. Reusability and Stability of the Catalyst

In this case, the stability and recyclability of the metal-supported catalyst were attempted using a soft heat regeneration treatment. To achieve this, the solid was recovered by filtration, being exhaustively washed with n-hexane and then with isopropanol. The resulting solid was dried at 60 °C overnight and calcined under air at 300 °C for 4 h to remove the traces of organic matter adsorbed on the catalyst. The resulting catalyst was hydrogenated at 400 °C for 3 h under H₂ flow (20 mL/min) using a 100 mL/min N₂ flow.

4. Conclusions

A series of nanosized Ru (1–2 wt. %)-based catalysts supported over tungstated zirconia WO_x/ZrO₂ (W/Zr) have been prepared and their activity and selectivity as catalysts have been studied during the hydrogenation of the fatty ester ethyl stearate into stearyl alcohol (octadecan-1-ol) in a batch reactor under different temperature and H₂ pressure conditions (175 °C and P_{H2} = 40 bar). The so-prepared catalysts have been characterized with a variety of analytical tools, confirming the higher dispersion of nanosized Ru over tungstated zirconia W/Zr and the higher reducibility of Ru species in comparison to pure zirconia according to an H₂-TPR study. In addition, an adequate Ru/W ratio will enhance the hydrogenating activity and selectivity towards the fatty alcohol C₁₈OH through a remarkable synergistic effect, which has been associated with the formation of WO₃ nanoparticles. This metal-Lewis acid cooperation between Ru/W could be evidenced by a significant exponential increase in the initial reaction rate (r₀) and the TOF for obtaining the fatty alcohol with the addition of W. We foresee that, in principle, the acidity of the catalyst could facilitate the reaction through a heterolytic hydrogen dissociation. In parallel,

the interaction of the ester group with W may cause a weakening or activation of the C=O bond, hence making the attack on the carbonyl group by the metal hydride (H^-) much easier. At the same time, the protonation (H^+) of the leaving alkoxy group would also be facilitated under acidic conditions, giving rise to the formation of the corresponding alcohol. Interestingly, the introduction of acidity by the W was not enough for the ester hydrolysis reaction to be competitive, so the formation of fatty alcohol from the hydrogenation of SA remained as a minority route. In this regard, we assumed that the ester hydrogenolysis, followed by aldehyde hydrogenation, was the main route towards the fatty alcohol formation (*versus* a minority pathway via carboxylic acid reduction). Finally, the catalyst was stable under the reaction conditions and reusable up to three times with no appreciable loss of activity and selectivity to 1-octadecanol.

We expect that the obtained insights into the active phase of $Ru-WO_x/ZrO_2$ can be a starting point that will facilitate the development of highly efficient and selective catalysts for the production of fatty alcohols from FAEs under mild and sustainable conditions.

Supplementary Materials: The following supporting information can be downloaded at: <https://www.mdpi.com/article/10.3390/catal13101362/s1>. Figure S1: XRP diffractograms obtained for W/Zr mixed oxides with increasing amounts of Ru: (a) Ru(0.5)/W(33)/Zr, (b) Ru(1.3)/W(33)/Zr and (c) Ru(2)/W(33)/Zr; Figure S2: XRP diffractograms of mixed oxide W/Ti and Ru-doped W/Ti mixed oxide: (a) W(30)/Ti, (b) Ru(1)/W(30)/Ti. (W: (▲) and TiO₂ Anatase (ρ)); Figure S3: TEM micrographs of the catalysts Ru(1)/Zr and Ru(1)/W(12)/Zr, with their average particle diameter (mean) and minimum and maximum particle diameter; Figure S4: TEM micrographs of the catalysts Ru(0.5)/W(33)/Zr and Ru(1.3)/W(33)/Zr with their average particle diameter (mean), minimum and maximum particle diameter; Figure S5: TEM micrographs of the catalysts Ru(2)/W(33)/Zr and Ru(1)/W(30)/Ti and their average particle diameter (mean) and minimum and maximum particle diameter.

Author Contributions: M.J.S.: conceptualization, funding acquisition, supervision, writing—original draft preparation; writing review and editing; D.Q.-R.: investigation, formal analysis; J.L.J.: investigation, formal analysis; M.C.: investigation, formal analysis. All authors have read and agreed to the published version of the manuscript.

Funding: This research was funded by the Ministry of Science and Innovation of the Spanish Government (grant number PGC2018-101247-B-100).

Data Availability Statement: Not applicable.

Acknowledgments: The work has been supported by the Ministry of Science and Innovation (Grant number PGC2018-101247-B-100). We also thank the Electron Microscopy Service of Universitat Politècnica de València for their help in the characterization of samples.

Conflicts of Interest: The authors declare no conflict of interest.

References

1. Richtler, H.J.; Knaut, J. Challenges to a mature industry: Marketing and economics of oleochemicals of Western Europe. *J. Am. Oil Chem. Soc.* **1984**, *61*, 160–175. [[CrossRef](#)]
2. Knaut, J.; Richtler, H.J. Trends in industrial uses of palm and lauric oils. *J. Am. Oil Chem. Soc.* **1985**, *62*, 317–327. [[CrossRef](#)]
3. Pritchard, J.; Filonenko, G.A.; Putten, R.; Hensen, E.J.M.; Pidko, E.A. Heterogeneous and homogeneous catalysis for the hydrogenation of carboxylic acid derivatives: History, advances and future directions. *Chem. Soc. Rev.* **2015**, *44*, 3808–3833. [[CrossRef](#)] [[PubMed](#)]
4. Sánchez, M.A.; Torres, G.C.; Mazzieri, V.A.; Pieck, C.L. Selective hydrogenation of fatty acids and methyl esters of fatty acids to obtain fatty alcohols—a review. *J. Chem. Tech. Biotech.* **2017**, *92*, 27–42. [[CrossRef](#)]
5. Chakraborty, S.; Dai, H.; Bhattacharya, P.; Fairweather, N.T.; Gibson, M.S.; Krause, J.A.; Guan, H. Iron-Based Catalysts for the Hydrogenation of Esters to Alcohols. *J. Am. Chem. Soc.* **2014**, *136*, 7869–7872. [[CrossRef](#)]
6. Clarke, M.L. Recent developments in the homogeneous hydrogenation of carboxylic acid esters. *Catal. Sci. Technol.* **2012**, *2*, 2418–2423. [[CrossRef](#)]
7. Srimani, D.; Mukherjee, D.A.; Goldberg, A.F.G.; Leitus, G.; Diskin-Posner, Y.; Shimon, L.J.W.; Ben David, Y.; Milstein, D. Cobalt-catalyzed hydrogenation of esters to alcohols: Unexpected reactivity trend indicates ester enolate intermediacy. *Angew. Chem. Int. Ed.* **2015**, *54*, 12357–12360. [[CrossRef](#)] [[PubMed](#)]

8. Spasyuk, D.; Vicent, C.; Gusev, D.G. Chemoselective Hydrogenation of Carbonyl Compounds and Acceptorless Dehydrogenative Coupling of Alcohols. *J. Am. Chem. Soc.* **2015**, *137*, 3743–3746. [[CrossRef](#)] [[PubMed](#)]
9. Otsuka, T.; Ishii, A.; Dub, P.A.; Ikariya, T. Practical Selective Hydrogenation of α -Fluorinated Esters with Bifunctional Pincer-Type Ruthenium(II) Catalysts Leading to Fluorinated Alcohols or Fluoral Hemiacetals. *J. Am. Chem. Soc.* **2013**, *135*, 9600–9603. [[CrossRef](#)] [[PubMed](#)]
10. Li, W.; Xie, J.H.; Yuan, M.L.; Zhou, Q.L. Ruthenium complexes of tetradentate bipyridine ligands: Highly efficient catalysts for the hydrogenation of carboxylic esters and lactones. *Green Chem.* **2014**, *16*, 4081–4085. [[CrossRef](#)]
11. Wang, F.; Tan, X.; Lv, H.; Zhang, X. New Ruthenium Complexes Based on Tetradentate Bipyridine Ligands for Catalytic Hydrogenation of Esters. *Chem. Asian J.* **2016**, *11*, 2103–2106. [[CrossRef](#)]
12. Pham, J.; Jarczyk, C.E.; Reynolds, E.F.; Kelly, S.E.; Kim, T.; He, T.; Keith, J.M.; Chianese, A.R. The key role of the latent N–H group in Milstein’s catalyst for ester hydrogenation. *Chem. Sci.* **2021**, *12*, 8477–8492. [[CrossRef](#)] [[PubMed](#)]
13. Fairweather, N.T.; Gibson, M.S.; Guan, H. Homogeneous Hydrogenation of Fatty Acid Methyl Esters and Natural Oils under Neat Conditions. *Organometallics* **2015**, *34*, 335–339. [[CrossRef](#)]
14. Singh, R.; Arora, A.; Singh, V. Biodiesel from oil produced in vegetative tissues of biomass—A review. *Bioresour. Technol.* **2021**, *326*, 124772. [[CrossRef](#)]
15. Chisti, Y. Biodiesel from microalgae. *Biotechnol. Adv.* **2007**, *25*, 294–306. [[CrossRef](#)] [[PubMed](#)]
16. Lestari, S.; Maki-Arvela, P.; Beltramini, J.; Max Lu, G.Q.; Murzin, D.Y. Transforming Triglycerides and Fatty Acids into Biofuels. *ChemSusChem* **2009**, *2*, 1109–1119. [[CrossRef](#)]
17. Korstanje, T.J.; Vlugt, J.I.; Elsevier, C.J.; Bruin, B. Hydrogenation of carboxylic acids with a homogeneous cobalt catalyst. *Science* **2015**, *350*, 298–302. [[CrossRef](#)] [[PubMed](#)]
18. Voeste, T.; Schmidt, H.; Marschner, F. Continuous Process of Producing Fatty Alcohols. U.S Patent 4259536A, 31 March 1981. Appl. No.: 100576.
19. Voeste, T.; Buchold, H. Production of fatty alcohols from fatty acids. *J. Am. Oil Chem. Soc.* **1984**, *61*, 350–352. [[CrossRef](#)]
20. Buchold, H. Natural fats and oils route to fatty alcohols. *Chem. Eng.* **1983**, *90*, 42–43.
21. Thakur, D.S.; Kundu, A. Catalysts for Fatty Alcohol Production from Renewable resources. *J. Am. Oil Chem. Soc.* **2016**, *93*, 1575–1593. [[CrossRef](#)]
22. Adkins, H.; Folkers, K. The catalytic hydrogenation of esters to alcohols. *J. Am. Chem. Soc.* **1931**, *53*, 1095–1097. [[CrossRef](#)]
23. Cant, N.W.; Trimm, D.L. The catalytic hydrogenolysis of esters to alcohols. *Catal. Rev.* **1994**, *36*, 645–683. [[CrossRef](#)]
24. Zhang, J.; Jiang, L.; Huang, H.; Tao, S.; Zhang, H.; Xiao, X.; Fang, J. Research Progress in Catalysts for Fatty Acid Ester Hydrogenation. *IOP Conf. Ser. Earth Environ. Sci.* **2020**, *571*, 012136. [[CrossRef](#)]
25. Fan, P.; Tang, M.X.; Jia, S.Y.; Du, M.X.; Qi, Y.Q.; Hou, X.L. Preparation of fatty alcohol by hydrogenation of fatty acid methyl esters at subcritical conditions. *China Surfactant Deterg. Cosmet.* **2011**, *41*, 408–410.
26. He, L.; Cheng, H.; Liang, G.; Yu, Y.; Zhao, F. Effect of structure of CuO/ZnO/Al₂O₃ composites on catalytic performance for hydrogenation of fatty acid ester. *Appl. Catal. A Gen.* **2013**, *452*, 88–93. [[CrossRef](#)]
27. Jiang, Z.; Fan, C.; Fan, M.; Zhang, P. Hydrogenation of methyl stearate to stearyl alcohol over Cu-based catalysts. *Petrochem. Technol.* **2016**, *45*, 1441–1448.
28. Jiang, Z.B.; Fan, M.M.; Zhang, P.B.; Jiang, B. Effect of dropping sequence on the preparation of Cu-Zn-Al-Ba catalyst for hydrogenation of fatty acid esters. *China J. Inorg. Chem.* **2016**, *32*, 1047–1054.
29. Huang, C.; Zhang, H.; Zhao, Y.; Chen, S.; Liu, Z. Journal of Colloid and Interface Science, Diatomite-supported Pd–M (M = Cu, Co, Ni) bimetal nanocatalysts for selective hydrogenation of long-chain aliphatic esters. *J. Colloid Interface Sci.* **2012**, *386*, 60–65. [[CrossRef](#)] [[PubMed](#)]
30. Liu, S.; Tan, S.; Li, W.; Song, J.; Yu, H.; Liu, Y.; Wu, Q. Hydrogenation of fatty acid methyl ester over Pd nanoparticles stabilized by thermoregulated ionic liquid. *Mol. Catal.* **2018**, *458*, 106–111. [[CrossRef](#)]
31. He, L.; Li, X.; Lin, W.; Li, W.; Cheng, H.; Yu, Y.; Fujita, S.; Arai, M.; Zhao, F. The selective hydrogenation of ethyl stearate to stearyl alcohol over Cu/Fe bimetallic catalysts. *J. Mol. Catal. A Chem.* **2014**, *392*, 143–149. [[CrossRef](#)]
32. Di, W.; Cheng, J.; Tian, S.; Li, J.; Chen, J.; Sun, Q. Synthesis and characterization of supported copper phyllosilicate catalysts for acetic ester hydrogenation to ethanol. *Appl. Catal. A Gen.* **2016**, *510*, 244–259. [[CrossRef](#)]
33. Yao, S.; Zhang, T.; Tang, X.; Li, D.; Zhang, W.; Lin, D.; Li, R.; Yan, H.; Liu, Y.; Feng, X.; et al. Octadecanol Production from Methyl Stearate by Catalytic Transfer Hydrogenation over Synergistic Co/HAP Catalysts. *Energy Fuels* **2021**, *35*, 9970–9982. [[CrossRef](#)]
34. Wang, L.; Niu, X.; Chen, J. SiO₂ supported Ni-In intermetallic compounds: Efficient for selective hydrogenation of fatty acid methyl esters to fatty alcohols. *Appl. Catal. B.* **2020**, *278*, 119293. [[CrossRef](#)]
35. Zhou, Y.; Remon, J.; Jiang, Z.; Matharu, A.V.; Hu, C. Tuning the selectivity of natural oils and fatty acids/esters deoxygenation to biofuels and fatty alcohols: A review. *Green Energy Environ.* **2023**, *8*, 722–743. [[CrossRef](#)]
36. Ni, J.; Leng, W.; Mao, J.; Wang, J.; Lin, J.; Jiang, D.; Li, X. Tuning electron density of metal nickel by support defects in Ni/ZrO₂ for selective hydrogenation of fatty acids to alkanes and alcohols. *Appl. Catal. B: Environ.* **2019**, *253*, 170–178. [[CrossRef](#)]
37. Luo, Z.; Bing, Q.; Kong, J.; Liu, J.; Zhao, C. Mechanism of supported Ru₃Sn₇ nanocluster-catalyzed selective hydrogenation of coconut oil to fatty alcohols. *Catal. Sci. Technol.* **2018**, *8*, 1322–1332. [[CrossRef](#)]

38. Sánchez, M.A.; Mazzieri, V.A.; Pronier, S.; Vicerich, M.A.; Especel, C.; Epron, F.; Pieck, C.L. Ru-Sn-B/TiO₂ catalysts for methyl oleate selective hydrogenation. Influence of the preparation method and the chlorine content. *J. Chem. Technol. Biotechnol.* **2019**, *94*, 982–991. [CrossRef]
39. Sánchez, M.A.; Mazzieri, V.A.; Oportus, M.; Reyes, P.; Pieck, C.L. Influence of Ge content on the activity of Ru-Ge-B/Al₂O₃ catalysts for selective hydrogenation of methyl oleate to oleyl alcohol. *Catal. Today* **2013**, *213*, 81–86. [CrossRef]
40. Gunstone, F.D.; Harwood, J.L.; Dijkstra, A.J. *The Lipid Handbook with CD-ROM*, 3rd ed.; CRC Press: Boca Raton, FL, USA, 2007; ISBN 0849396883/ISBN 978-0849396885.
41. Auxeméry, A.; Frias, B.B.; Smal, E.; Dziadek, K.; Philippot, G.; Łęgutko, P.; Simonov, M.; Thomas, S.; Adamski, A.; Sadykov, V.; et al. Continuous Supercritical Solvothermal Preparation of Nanostructured Ceria-Zirconia as Supports for Dry Methane Reforming Catalysts. *J. Supercrit. Fluids* **2020**, *162*, 104855. [CrossRef]
42. Sunita, G.; Devassy, B.M.; Vinu, A.; Sawant, D.P.; Balasubramanian, V.; Halligudi, S. Synthesis of biodiesel over zirconia-supported isopoly and heteropoly tungstate catalysts. *Catal. Commun.* **2008**, *9*, 696–702. [CrossRef]
43. Lee, J.H.; Shin, C.H.; Suh, Y.W. Higher Brønsted acidity of WO_x/ZrO₂ catalysts prepared using a high-surface-area zirconium oxyhydroxide. *Mol. Catal.* **2017**, *438*, 272–279. [CrossRef]
44. Soultanidis, N.; Zhou, W.; Psarras, A.C.; Gonzalez, A.J.; Iliopoulou, E.F.; Kiely, C.J.; Wachs, I.E.; Wong, M.S. Relating n-pentane isomerization activity to the tungsten surface density of WO_x/ZrO₂. *J. Am. Chem. Soc.* **2010**, *132*, 13462–13471. [CrossRef]
45. Garcia-Perez, D.; Alvarez-Galan, M.C.; Campos-Martin, J.M.; Fierro, J.L.G. Influence of the Reduction Temperature and the Nature of the Support on the Performance of Zirconia and Alumina-Supported Pt Catalysts for n-Dodecane Hydroisomerization. *Catalysts* **2021**, *11*, 88. [CrossRef]
46. Li, M.; Chen, Z. Epoxidation of the polyisobutene using WO₃/ZrO₂ catalyst. *Res. Chem. Intermed.* **2012**, *38*, 1921–1929. [CrossRef]
47. Gauna, M.R.; Conconi, M.S.; Gomez, S.; Suárez, G.; Aglietti, E.F.; Rendtorff, N.M. Monoclinic-tetragonal zirconia quantification of commercial nanopowder mixtures by XRD and DTA. *Ceramics-Silikáty* **2015**, *59*, 318–325.
48. Rodina, V.O.; Ermakov, D.Y.; Saraev, A.A.; Reshetnikov, S.I.; Yakovlev, V.A. Influence of reaction conditions and kinetic analysis of the selective hydrogenation of oleic acid toward fatty alcohols on Ru-Sn-B/Al₂O₃ in the flow reactor. *Appl. Catal. B Environ.* **2017**, *209*, 611–620. [CrossRef]
49. Fonseca Benítez, C.A.; Mazzieri, V.A.; Vera, C.R.; Benitez, V.M.; Pieck, C.L. Selective hydrogenation of oleic acid to fatty alcohols over a Rh-Sn-B/Al₂O₃ catalyst: Kinetics and optimal reaction conditions. *React. Chem. Eng.* **2021**, *6*, 726–746. [CrossRef]
50. Catlow, C.R.A.; Chadwick, A.V.; Greaves, G.N.; Moroney, L.M. EXAFS Study of Yttria-Stabilized Zirconia. *J. Am. Ceram. Soc.* **1986**, *69*, 272–277. [CrossRef]
51. Li, P.; Chen, I.-W.; Penner-Hahn, J.E. X-Ray-Absorption Studies of Zirconia Polymorphs. II. Effect of Y₂O₃ Dopant on ZrO₂ Structure. *Phys. Rev. B Condens. Matter Mater. Phys.* **1993**, *48*, 10074–10081. [CrossRef] [PubMed]
52. Li, P.; Chen, I.-W.; Penner-Hahn, J.E. Effect of Dopants on Zirconia Stabilization-An X-Ray Absorption Study: I, Trivalent Dopants. *J. Am. Ceram. Soc.* **1994**, *77*, 118–128. [CrossRef]
53. Patil, M.K.; Prasad, A.N.; Reddy, B.M. Zirconia-Based Solid Acids: Green and Heterogeneous Catalysts for Organic Synthesis. *Curr. Org. Chem.* **2011**, *15*, 3961–3985. [CrossRef]
54. Song, K.; Zhang, H.; Zhang, Y.; Tang, Y.; Tang, K. Preparation and characterization of WO_x/ZrO₂ nanosized catalysts with high WO_x dispersion threshold and acidity. *J. Catal.* **2013**, *299*, 119–128. [CrossRef]
55. Thamaphat, K.; Limsuwan, P.; Ngotawornchai, B. Phase Characterization of TiO₂ Powder by XRD and TEM. *Agric. Nat. Resour.* **2008**, *42*, 357–361. Available online: <https://li01.tci-thaijo.org/index.php/anres/article/view/244620> (accessed on 20 August 2023).
56. Sun, G.; Xu, A.; He, Y.; Yang, M.; Du, H.; Sun, C. Ruthenium catalysts supported on high-surface-area zirconia for the catalytic wet oxidation of N,N-dimethyl formamide. *J. Hazard. Mater.* **2008**, *156*, 335–341. [CrossRef] [PubMed]
57. Jayat, F.; Sabater, M.J.; Rohan, D.; Guisnet, M. Acylation of aromatics over a HBEA Zeolite. Effect of solvent and of acylating agent. *Stud. Surf. Sci. Catal.* **1997**, *108*, 91–98.
58. Adam, W.; Corma, A.; Miranda, M.A.; Sabater, M.J.; Sahin, C. Photochemical and chemical electron transfer reactions of bicyclo[2.1.0]pentanes (housanes) in solution and in zeolite cavities. *J. Am. Chem. Soc.* **1996**, *118*, 2380–2386. [CrossRef]
59. Cerro, M.; Iborra, S.; Martínez, C.; Sabater, M.J.; Corma, A. Methanolysis of sunflower oil using gem-diamines as active organocatalysts for biodiesel production. *Appl. Catal. A Gen* **2010**, *382*, 36–42. [CrossRef]
60. Tamura, M.; Nakagawa, Y.; Tomishige, K. Recent developments of heterogeneous catalysts for hydrogenation of carboxylic acids to their corresponding alcohols. *Asian J. Org. Chem.* **2020**, *9*, 126–143. [CrossRef]
61. Zhao, K.; Han, W.; Tang, Z.; Zhang, G.; Lu, J.; Lu, G.; Zhen, X. Investigation of coating technology and catalytic performance over monolithic V₂O₅-WO₃/TiO₂ catalyst for selective catalytic reduction of NO_x with NH₃. *Colloids Surf. A Physicochem. Eng. Asp.* **2016**, *503*, 53–60. [CrossRef]
62. Lopez-Prado, M.V.; Sabater, M.J.; Corma, A. A Bifunctional Metal/Acid Catalyst for One-pot Multistep Synthesis of Pharmaceuticals. *Petrol. Chem.* **2020**, *60*, 499–507. [CrossRef]
63. Bonds, G.C. *Metal-Catalysed Reactions of Hydrocarbons*; Springer: New York, NY, USA, 2005.
64. Corma, A.; Sabater, M.J. *Gold Catalysis for Hydrogenation Reactions*; RSC Catalysis Series; RSC: London, UK, 2013; Volume 13, pp. 146–200, ISBN 978-1-84973-571-1. [CrossRef]

65. Kazansky, V.B.; Subbotina, I.R.; van Santen, R.A.; Hensen, E.J.M. DRIFTS study of the chemical state of modifying gallium ions in reduced Ga/ZSM-5 prepared by impregnation: I. Observation of gallium hydrides and application of CO adsorption as a molecular probe for reduced gallium ions. *J. Catal.* **2004**, *227*, 263–269. [[CrossRef](#)]
66. Barton, D.G.; Soled, S.L.; Iglesia, E. Solid acid catalysts based on supported tungsten oxides. *Top. Catal.* **1998**, *6*, 87–99. [[CrossRef](#)]
67. Calabro, D.C.; Vartuli, J.C.; Santiesteban, J.G. The characterization of tungsten-oxide-modified zirconia supports for dual functional catalysis. *Top. Catal.* **2002**, *18*, 231–242. [[CrossRef](#)]

Disclaimer/Publisher’s Note: The statements, opinions and data contained in all publications are solely those of the individual author(s) and contributor(s) and not of MDPI and/or the editor(s). MDPI and/or the editor(s) disclaim responsibility for any injury to people or property resulting from any ideas, methods, instructions or products referred to in the content.